ANL-7320

ANL-7320

Conf-661019--

ARGONNE NATIONAL LABORATORY

MASTER

PROCEEDINGS OF THE INTERNATIONAL CONFERENCE ON FAST CRITICAL EXPERIMENTS AND THEIR ANALYSIS

October 10-13, 1966

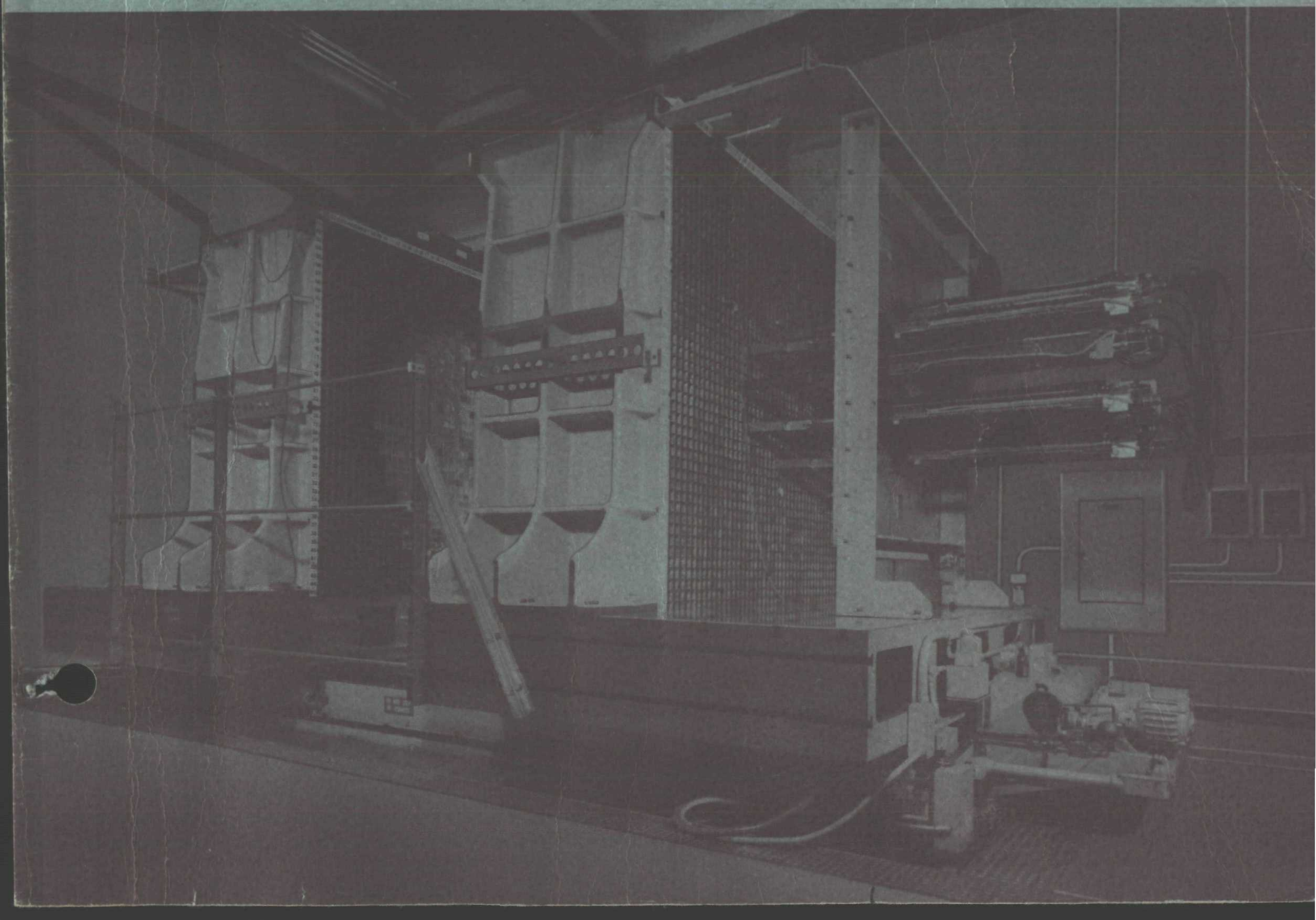

The facilities of Argonne National Laboratory are owned by the United States Government. Under the terms of a contract (W-31-109-Eng-38) between the U. S. Atomic Energy Commission, Argonne Universities Association and The University of Chicago, the University employs the staff and operates the Laboratory in accordance with policies and programs formulated, approved and reviewed by the Association.

Printed in the United States of America
Available from
Clearinghouse for Federal Scientific and Technical Information
National Bureau of Standards, U. S. Department of Commerce
Springfield, Virginia 22151
Price: Printed Copy $3.00; Microfiche $0.65

Presented by A. B. Reynolds

Application of the SEFOR Critical Experiments at ZPR-3 to SEFOR

A. B. REYNOLDS AND S. L. STEWART

Advanced Products Operation
General Electric Company
San Jose, California

ABSTRACT

A series of critical experiments was performed with a mockup of SEFOR at ZPR-3. Analyses of these experiments and the application of the results to the SEFOR design are discussed.

Values of the critical mass were determined for 1-, 2-, and 3-segment SEFOR fuel designs in order to help establish the plutonium atom fraction in the SEFOR fuel.

Reactivity effects of axial fuel expansion were measured which led to selection of the 2-segment design for SEFOR.

Measurements of the reactivity worth of the radial reflector established the adequacy of the SEFOR reflector-control system.

The Doppler coefficient was measured. The calculated U^{238} Doppler coefficient was in agreement with the experimental value; the measured Pu^{239} contribution to the SEFOR Doppler coefficient was near zero. It was demonstrated that the SEFOR Doppler coefficient $[T(dk/dT) = -0.0085]$ is significantly more negative than the conservative value assumed for safeguards analysis.

The maximum positive reactivity due to loss of sodium was measured; the measured reactivity was small (+6¢) and close to the calculated value.

The ratio of prompt-neutron lifetime to delayed-neutron fraction was measured both by the pulsed neutron technique and by noise analysis. The values measured by the two techniques were in agreement, and, for a calculated β_{eff} of 0.0033, gave $l = 0.68$ μsec.

Fission ratios, fission and boron traverses, and plutonium worth distributions were measured and compared with calculations.

1. Introduction

SEFOR (Southwest Experimental Fast Oxide Reactor) is a 20-MW(t) fast-spectrum reactor fueled with PuO_2-UO_2 and cooled with sodium. SEFOR will have characteristics similar to the large, soft-spectrum fast breeder reactors fueled with mixed PuO_2-UO_2. SEFOR will be used to obtain physics and engineering data at fuel compositions, temperatures, and crystalline states characteristic of operating conditions of power reactors. SEFOR is particularly designed for the systematic determination of the Doppler coefficient of reactivity at temperatures up to the vicinity of fuel melting.

The SEFOR Project consists of two major parts: the design and construction of the reactor, and a related research and development program. Funds for the design and construction of the facility are being provided by the Southwest Atomic Energy Associates (a group of seventeen investor-owned utility companies located in the South and Southwest part of the United States), together with the Karlsruhe Laboratory of the Federal Republic of Germany, EURATOM, and the General Electric Company. The United States Atomic Energy Commission is supporting the Research and Development Program.

This report describes work performed as part of the Research and Development Program. A series of experiments was conducted on a mockup of SEFOR in the ZPR-3 facility in a joint program by the General Electric Company and Argonne National Laboratory. Criticality of the mockup was achieved November 17, 1965; the experimental program was conducted from October 1965 to April 1966. Reference 1 provides a description of the experiments and experimental results. The present report gives an analysis of these results and describes how they are applied to the SEFOR design. Further details of the analysis are presented in Ref. 2.

The following experiments were performed on the SEFOR mockup:

1. critical mass for 1-, 2-, and 3-segment core designs;
2. reactivity of axial fuel expansion for 1-, 2-, and 3-segment designs;
3. worth of reflector control;
4. Doppler coefficient;
5. sodium-loss reactivity;

6. ratio of prompt-neutron lifetime to effective delayed-neutron fraction, l/β_{eff};
7. fission ratios and reaction-rate distributions.

2. Description of the Mockup

2.1. *Characteristics of SEFOR of Significance to the Mockup Design*

A brief description of SEFOR will provide a basis for discussion of the mockup. A more complete description is given in Ref. 3. The SEFOR fuel rods are composed of two fuel segments with a gap between the segments into which fuel can expand axially. The purpose of this segmented fuel design is to reduce the reactivity effect due to axial expansion, as described further in Sect. 4. The active fuel height is 85.9 cm and the effective core diameter 88.2 cm.

The reactor is controlled by movement of the 6-in.-thick radial nickel reflector; the reflector is divided into 10 segments which can be withdrawn, leaving a nearly completely voided reflector region. Behind the SEFOR reflector is a 2-in. neutron shield region containing boron carbide, followed by a serpentine neutron shield.

Between the core and the radial reflector are a sodium downcomer region, the steel reactor vessel, and a steel shroud. Above and below the core are axial reflectors in which nickel replaces fuel.

After the ZPR-3 experimental program was completed, an additional change was made in the SEFOR core design—in particular, the BeO volume fraction was reduced. The volume fractions (not including the gap) are given in Table 1 for both the final SEFOR design and the design represented by the mockup.

2.2. *Geometry and Composition of the Mockup*

Core dimensions and compositions were chosen to mock up the SEFOR core at 350°F, which is approximately the temperature for refueling and for the initial wet critical for SEFOR.

One purpose of the mockup was to facilitate the choice of the number of fuel segments for the SEFOR design. Therefore, experiments to measure critical mass and axial expansion were made for 1-, 2-, and 3-segment core mockups.

TABLE 1. SEFOR VOLUME FRACTIONS

Material	Final Design	Mockup Design
Fuel	0.432	0.429
Sodium	0.295	0.303
Steel	0.216	0.182
BeO	0.057	0.086

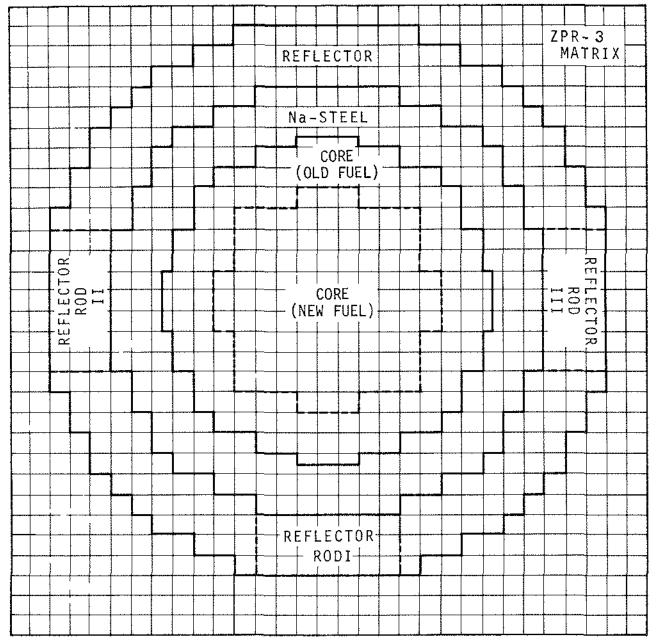

FIG. 1. Interface View of SEFOR Mockup Assembly 47A, Loading 15.

A cross-sectional view and an elevation view of the 1-segment mockup are shown in Figures 1 and 2. For the 2- and 3-segment mockups, the radius of the inner core was increased to 33.8 cm. The increase in core heights for the 2- and 3-segment mockups and location of the gaps are described in Sect. 4 (see Figures 6 and 7). The average compositions of each region for the 1-, 2-, and 3-segment mockups are given in References 1 and 2. Details of the drawer loadings are presented in Ref. 1.

Criticality was achieved first with 1-segment Assembly 47, Loading 15. This assembly is described in Ref. 4 and was chosen for analysis in Ref. 5 since it had the cleanest (i.e., simplest and most uniform) geometry. The 1-segment experiments analyzed in the present report were made with Assembly 47A, Loading 15 in which additional sodium was placed between the core and reflector, the nickel from two simulated reflector control rods was removed, and the ZPR-3 control rods were spiked further to add to the operating reactivity margin.

2.3. *Oxygen Mockup*

The SEFOR fuel is UO_2-PuO_2. The ZPR-3 fuel is metallic plutonium, uranium, and Pu-U alloy. Therefore it was necessary to mock up in ZPR-3 the oxygen in the SEFOR fuel.

The oxygen was mocked up by a combination of oxygen in sodium carbonate (Na_2CO_3), carbon in

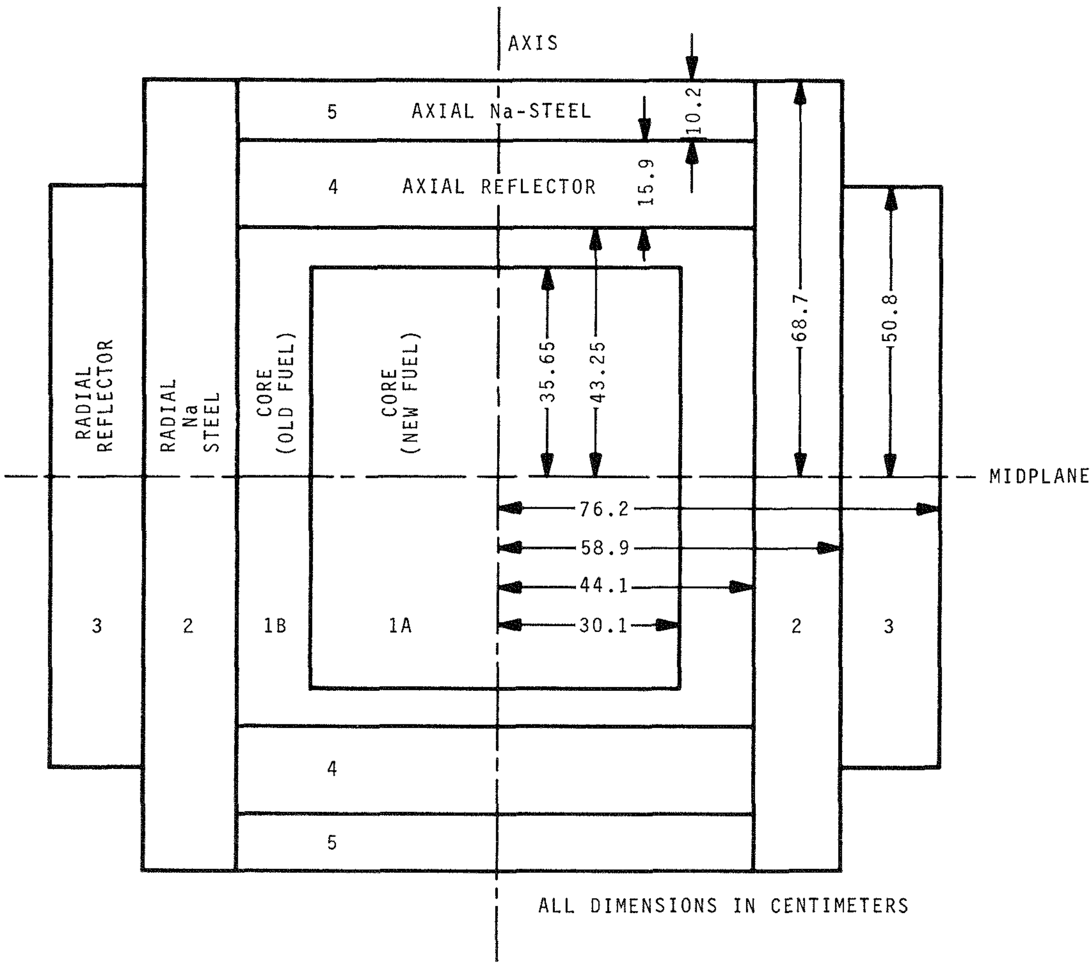

FIG. 2. Elevation View of SEFOR Mockup Assembly 47A, Loading 15.

Na_2CO_3, and aluminum.* The mockup contained 0.525 atom of oxygen, 0.175 of carbon, and 0.388 of aluminum per atom of oxygen in the SEFOR fuel.

The oxygen affects the core design primarily through its influence on leakage and neutron spectrum. In order to assess the effectiveness of the oxygen mockup, pre-experimental leakage and spectrum calculations were made for the SEFOR core at 350°F (hence, with the correct amount of oxygen) and for the mockup in ZPR-3 with the oxygen mocked up by oxygen, carbon, and aluminum. These results are given in Table 2.

TABLE 2. EFFECTIVENESS OF OXYGEN MOCKUP

	Actual Oxygen	Oxygen Mockup
Criticality factor	1.0041	1.0043
Leakage Probability		
Radial	0.234	0.230
Axial	0.092	0.090
Fraction of Fissions below 9 keV	0.203	0.198

3. Plutonium Atom Fraction

The plutonium atom fraction in the SEFOR fuel was based on calculations normalized to critical mass calculations of the SEFOR mockup. The procedure for establishing the plutonium atom fraction included the following steps:

1. calculation of criticality factors for the SEFOR mockup and for SEFOR, using identical methods;
2. normalization of the calculation of the SEFOR criticality factor by the ratio of the calculated and experimental criticality factors for the SEFOR mockup;
3. establishment of the design criticality factor for 20-MW operation for SEFOR;
4. adjustment of the SEFOR plutonium atom fraction to obtain the design criticality factor.

* This mockup for oxygen was proposed by the Karlsruhe Laboratory of the Federal Republic of Germany which is participating in the SEFOR Project.

TABLE 3. CALCULATED CRITICALITY FACTORS FOR MOCKUP
(*Calculated Values Are to be Compared with Experimental Values of Unity*)

Loading	Calculational Model	Calculated Criticality Factor
1-segment	2-dimensional (r,z), 4-group	0.985
2-segment	2-dimensional (r,z), 4-group	0.977
3-segment	2-dimensional (r,z), 4-group	0.974

3.1. Criticality Calculations for SEFOR Mockup

Criticality calculations were made for the 1-segment, 2-segment, and 3-segment SEFOR mockups. Diffusion theory was used throughout. Calculations included 4-group, 2-dimensional (r, z) and 18-group, 1-dimensional (both radial and axial) calculations. Four-group* and 18-group cross sections were condensed from 60-group cross sections in each important region, using 60-group, 1-dimensional calculations in both the radial and axial directions. The PDQ code was used for 2-dimensional calculations; the DEMON code was used for 1-dimensional calculations. The 60-group cross-section set used was based on the 1965 60-group General Electric set.[4, 7]

The results of the 2-dimensional calculations for each of the critical loadings are given in Table 3. It was learned during the early analysis of the segmented core mockups that the use of 18-group, 1-dimensional axial calculations introduced considerable uncertainty in the radial leakage at the gaps. Therefore, greater reliance was placed on the use of the 2-dimensional calculations, together with space-dependent condensation of 60-group cross sections to four groups.

Small corrections to the criticality calculations were necessary since all the nickel in the reflector and all the ZPR-3 control rods were assumed to be inserted for the computer calculations, whereas some of the nickel and control rods were removed in the actual critical loadings for the mockups in ZPR-3. The worth of the removed nickel and control rods in the 1-segment loading was $\Delta k/k = 0.0073$; the worth in the 2-segment loading was $\Delta k/k = 0.0042$; the worth in the 3-segment loading was $\Delta k/k = 0.0007$. These corrections have been taken into account in the results listed in Table 3 so that the values in Table 3 should be compared with the experimental values of unity.

Shelf-shielding at low energy was accounted for by Bell's technique[8] for applying the rational approximation to a repeating lattice. No corrections were made for high-energy heterogeneity effects in either the mockup or the SEFOR criticality calculations. Additional corrections due to the gap between the two halves of the ZPR-3, the noncylindrical surface of the core, and streaming parallel to the plates of materials in the mockup are of little significance.[6]

* The lower energies of groups 1, 2, and 3 for the 4-group structure were 1.35 MeV, 180 keV, and 9.1 keV, respectively.

The value of 0.985 for the criticality factor of the 1-segment core is consistent with those calculations of the initial SEFOR mockup loading reported in Ref. 5 which were based on the same cross-section data used in the SEFOR program. A new set of cross sections is recommended in Ref. 5 which gives much closer agreement with the initial loading.

It is noted from Table 3 that the reactivity effect of the gap is overestimated. From comparison of the critical masses of the 1-, 2-, and 3-segment mockups, it is estimated that the reactivity effect of the gap in the 2-segment mockup was -2.25% $\Delta k/k$ and that the combined reactivity of the gaps in the 3-segment mockup was -4.5% $\Delta k/k$. The 2-dimensional results in Table 3 indicate -3.0% and -5.6% reactivities for the gaps for the 2- and 3-segment mockups, respectively.

Several sources for the uncertainty in the treatment of the gap are possible. Diffusion theory may be inadequate for the accurate calculation of leakage at the gaps; transport approximations may provide better agreement. The use of additional neutron groups in a diffusion theory code may provide better agreement. For the results reported in Table 3, all materials in the gap were homogenized to obtain atom densities in the gap. Slightly different criticality factors are obtained for different gap models—for example, a gap model in which the gap is separated into three axial regions or a model in which a small section of the core is homogenized with the gap.

3.2. Design Criticality Factor for SEFOR

SEFOR is designed to reach a power level of 20 MW with a fixed core diameter with fuel rods of a single atom fraction of plutonium. A reasonable margin of error must be allowed for the extrapolation from the mockup in ZPR-3 to SEFOR at 20 MW.

Moreover, a second core (Core II) will replace the first core (Core I) later in the SEFOR experimental program. Although the specific design for Core II is not fixed, various designs being considered involve removal of the BeO (to harden the spectrum) with an accompanying loss in reactivity in the range of 1.5% to 2.5% in $\Delta k/k$.

These considerations led to the choice of a design criticality factor of $k = 1.035$. This allows a 1.0 to 2.0% margin for overestimating the criticality factor at 20 MW of Core I together with a margin of 1.5 to 2.5% reactivity loss for the change in Core II.

3.3. Calculations of SEFOR Plutonium Atom Fraction

The 2-segment design was chosen for SEFOR. In order to select the fuel atom fraction of plutonium for the SEFOR fuel, 4-group, 2-dimensional, and 18-group axial calculations of SEFOR are being made using the same techniques used for the ZPR-3 criticality calculations. The calculated SEFOR criticality factors are normalized by the ratio of the experimental to calculated values given in Table 3.

Uranium-238 cross sections in SEFOR were calculated for the average fuel temperature at 20 MW and 1400°K, using the same techniques used for the room-temperature ZPR-3 mockup. For Pu^{239}, room-temperature cross sections are used in the 20-MW SEFOR calculations since the ZPR-3 experiments, in verification of earlier experiments, showed almost zero Doppler contribution from Pu^{239}.

4. Reactivity Effect of Axial Fuel Expansion

The quantities that will be measured in the SEFOR Doppler experiments will be power and energy coefficients of the fuel, from which will be calculated fuel temperature coefficients. The fuel temperature coefficient will include two components—the Doppler effect and the axial fuel-expansion effect. In order to obtain the Doppler effect, it is necessary to subtract the calculated value of the effect of axial fuel expansion from the total fuel-reactivity effect. Therefore, the accuracy of the measured Doppler coefficient is strongly influenced by the accuracy with which the effect of axial fuel expansion can be calculated.

With no special provisions in the fuel design to reduce the axial expansion effect, this effect in SEFOR would be almost as large as the Doppler effect. Therefore, two techniques are being incorporated in the SEFOR fuel design to reduce the axial expansion effect—dishing the ends of the fuel pellets, and segmenting the fuel.

To help in the selection of the SEFOR fuel design and to check calculational techniques, axial-expansion reactivity was measured for designs with 1, 2, and 3 segments.

4.1. Design of ZPR-3 Experiments

4.1.1 Selection of Experiments

For segmented fuel there exist two principal components to the effect of axial fuel expansion: a large negative component due to increased radial leakage in the fuel regions when the fuel expands, and a large positive component due to decreased radial leakage in the gap regions as the gap thickness is decreased. It was important to measure each of these two components independently to check the calculational method for each effect and to measure them together to see if the effects are superposable.

Measurement of the effect of axial fuel expansion in the 1-segment core provided an independent measure of the first component. Decreasing the thickness of a gap while not expanding the fuel provided an independent measure of the second component; this was carried out for the larger gap in the 3-segment mockup. In addition, the effects of simultaneous expansion of fuel and compaction of the gaps were measured for both the 2- and the 3-segment mockups. Total fuel expansion in all cases was ½ inch. The gap in the 2-segment mockup was closed ⅜ inch. The upper gap in the 3-segment mockup was closed ¼ inch; the lower gap was closed ⅛ inch.

The gap thickness was the same at all radial positions in the mockup. In SEFOR there will be a radial distribution both of the gap thickness and of the change in gap thickness with a change in power due to the radial distribution in fuel temperature. Hence, in some of the ZPR-3 expansion experiments, the inner (new) fuel zone was completely expanded before any of the outer (old) fuel zone in order to obtain information on the radial dependence of the axial-expansion effect that could be compared with a calculational model.

4.1.2 Gap Mockup

It was recognized early that the gap mockup in ZPR-3 must accurately represent the important geometrical characteristics of the gap in SEFOR. This meant that the axial distribution of the void and other materials in the gap between the fuel segments in SEFOR must be mocked up in ZPR-3 in order to assure that the streaming effects were measured correctly.

Schematic drawings of the gap in the 2-segment SEFOR design and the gap mockup in ZPR-3 are shown in Figures 3 and 4. Figure 3 shows the gap with the fuel unexpanded; Figure 4 shows the same gap with fuel expanded. This gap mockup describes well the geometrical distribution of material in the SEFOR gap. The material in the gap mockup was located in adjacent drawers in such a way that no straight-through streaming paths were present, thereby mocking up the correct situation for SEFOR.

4.1.3 Mockup of Expansion

To mock up expansion of the fuel, ⅛-in. aluminum spacers were located between fuel plates. All experiments mocked up an expansion of ½ in.; hence, four spacers were required. Later, the reactivity effect of the aluminum spacers was measured. This method of expansion differs from that in SEFOR in that the expansion occurs throughout the length of the fuel rod in SEFOR, the expansion being proportional to the change in fuel temperature in the axial direction. However, the mockup calculations account for the discrete placement of the spacers, and the error due to this difference between the mockup and SEFOR is not considered to be significant.

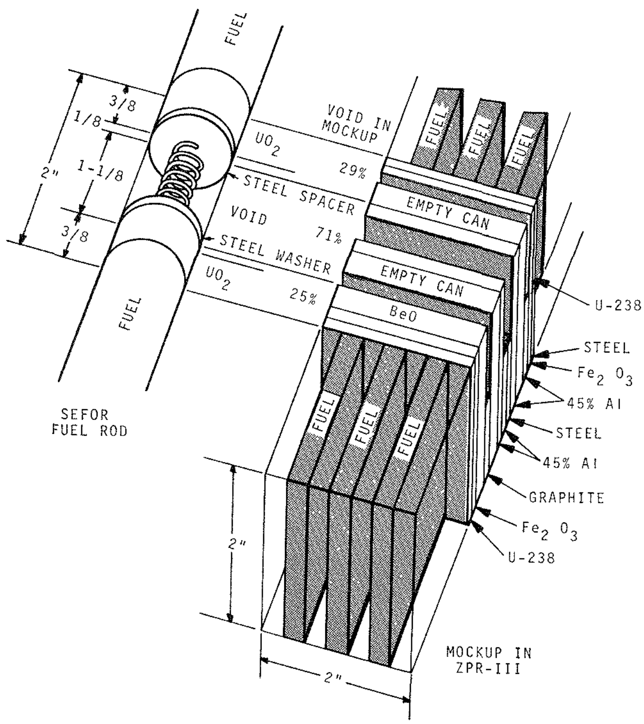

FIG. 3. Gap Mockup in ZPR-3 (Fuel Unexpanded).

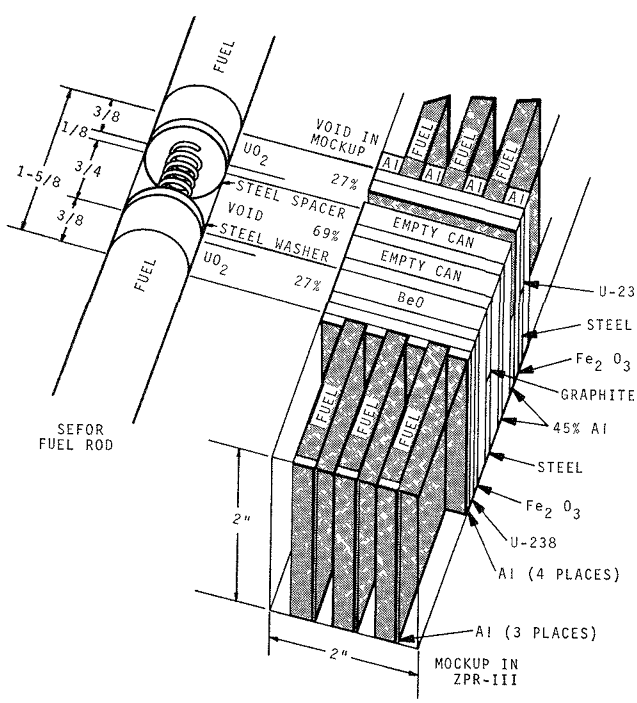

FIG. 4. Gap Mockup in ZPR-3 (Fuel Expanded).

The locations of the aluminum spacers for the 1-, 2-, and 3-segment experiments are given in Figures 5, 6, and 7, together with dimensions before and after expansion.

Treatment of the expansion of the fuel into the gap was shown in Fig. 4. It is noted that aluminum spacers are placed in the spaces at the ends of the non-fuel columns adjacent to the gap. To reduce the uncertainty introduced by this aluminum, a very nearly equal amount of aluminum was removed from the center part of the gap to accommodate the fuel expansion. Thus the total aluminum in and immediately around the gap remained nearly constant before and after the expansion.

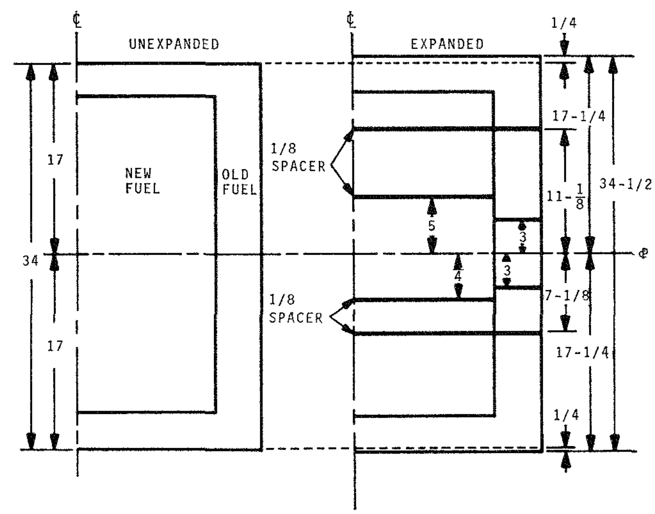

FIG. 5. Expansion Experiment in One-segment Mockup (Dimensions in Inches).

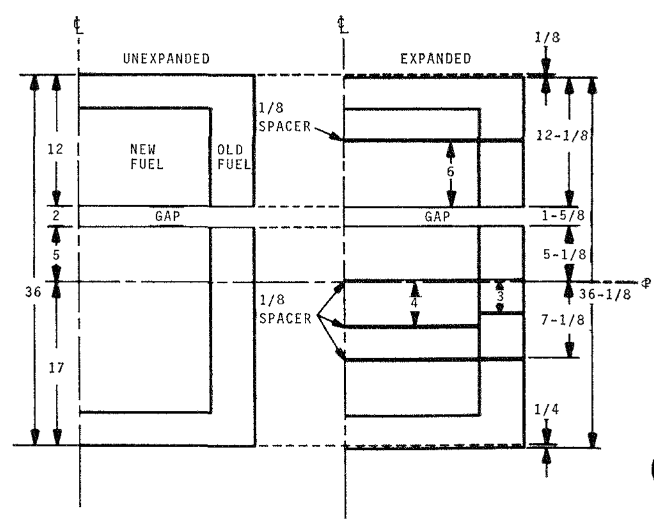

FIG. 6. Expansion Experiment in 2-segment Mockup (Dimensions in inches).

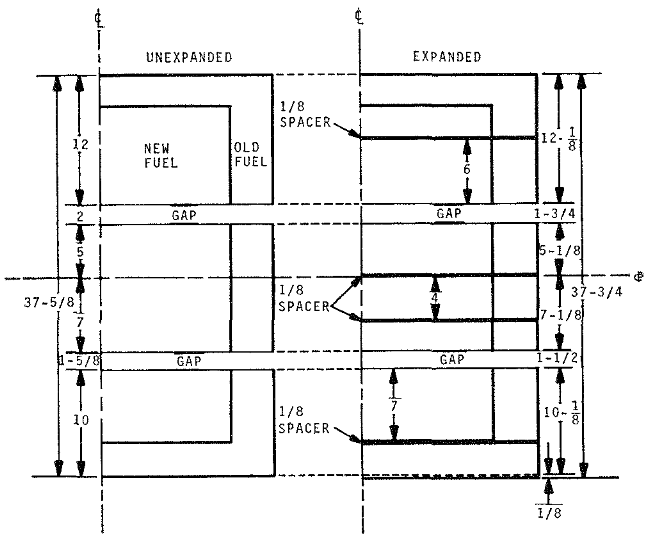

FIG. 7. Expansion Experiment in 3-segment Mockup (Dimensions in Inches).

4.2. Results

Experimental and calculated results are compared in Table 4.

The experimental results show clearly the efficacy of segmenting the fuel. Observation of the results of the 1-segment experiment and the 3-segment experiment in which only the gap thickness was changed shows the compensating effects that take place during a power change with segmented fuel. The two compensating components appear to be approximately superposable. For example, it is reasonable to estimate that if the lower gap of the 3-segment core had been closed ⅛ in. in addition to closing the upper gap ¼ in., the combined reactivity effect of changing the gap thicknesses only would be $\sim$+\$1.1. Combined with the −\$1.4 value for the effect of fuel expansion alone gives −\$0.3 for the net effect, which compares well the measured value of −\$0.2.

It is also reasonable (as indicated by the experiments) that the effect of the ⅜-in. decrease in gap thickness for the 2-segment case is less than the combined decrease in the gap thicknesses for the 3-segment case. The reason is that the gap in the 2-segment case skews the flux toward the bottom part of the core, thus decreasing the importance of the gap location in the 2-segment case relative to the 3-segment case.

The calculated results differ significantly with the experimental values. The fuel-expansion component (1-segment case) was calculated to be 21% larger than that experimentally observed. The gap-compaction component (3-segment, gap-only case) was calculated to be 36% higher than observed in the experiment. These errors combine in a fortuitous way to give close agreement for the 2-segment case. Normalization of the present diffusion-theory calculational method to the ZPR-3 results provides a technique which is sufficiently accurate for the SEFOR experimental program, however, since the magnitude of the axial-expansion effect is reduced so much by the combined techniques of dishing the pellets and using 2-segment fuel.

The results in Table 4 have been corrected for removal of the aluminum spacers used to expand the fuel in the mockup. The effect of removal of the aluminum was measured experimentally. The size of this correction and comparisons with calculations are shown in Table 5.

4.3. Calculational Model

The calculations were made by 2-dimensional, 4-group diffusion theory using PDQ. Four-group cross sections were condensed from the SEFOR-mockup 60-group set for each important region using 1-dimensional radial and axial problems. All materials in the gap were homogenized to obtain atom densities in the gap. Homogenizing a small section of the core with the gap gave results slightly closer to experiment; separating the gap into three axial regions gave results which disagreed further from the experiment. Care was taken in mocking up exact compositions and dimensions, and accounting for the presence of control drawers, variations in fuel plate locations, and details of the fuel plate design at the gap-fuel interface. For each calculation, material balances were checked before and after expansion to assure that material was not inadvertently added or lost; this was important since some problems contained as many as 50 regions.

TABLE 4. Reactivity duel to Axial Fuel Expansion

Segments		Experimental (\$)	Calculated (\$)
1	Fuel expanded	−1.39 ± 0.04	−1.68
2	Fuel expanded	−0.46 ± 0.02	−0.49
	Fuel expanded in inner fuel region only	−0.37 ± 0.02	−0.36
3	Fuel expanded	−0.20 ± 0.02	−0.04
	Upper gap thickness decreased only (no accompanying fuel expansion)	+0.74 ± 0.02	+1.01

TABLE 5. Effect of Aluminum Spacers
($\Delta k/k$ *for Removal of Aluminum Spacers*)

Case	Experimental, ¢	Calculated, ¢
1-segment	−5	−7
2-segment	−7	−6
3-segment	−4	Not calculated

5. Reflector Control Worth

The reactivity effect of the reflector of the SEFOR mockup was measured in order to evaluate the worth of the SEFOR control system. The value obtained for the SEFOR control worth was \$(11 ± 2). This value compares with the predicted operating control requirement for SEFOR of \$5.5. The large difference between the \$11 control worth and the \$5.5 operating requirement insures adequate availability of shutdown reactivity.

In this section the experimental procedures and results are described, together with two methods used to obtain the SEFOR reflector worth from the ZPR-3 measurements. It was not feasible to measure the worth of a segment of the reflector larger than one quadrant. Therefore, calculations were necessary to provide an extrapolation to the total SEFOR reflector worth.

5.1. Experimental Procedure

The reactivity effects of removing both one-tenth and one-fourth of the nickel from the ZPR-3 reflector were measured in order to simulate approximately the withdrawal of one of the ten SEFOR reflector control rods and a quadrant of the SEFOR reflector.

The single reflector-rod measurement was made by the rod-swap technique. The nickel from 21 of the 236 drawers in the reflector region of Fig. 1 was removed in small increments. The reactivity effect of each increment was measured by compensation with a calibrated ZPR-3 control rod. The nickel removed in each increment was placed in a reflector position on a different side of the core before removal of the next increment.

The worth of one quadrant was determined both by subcritical multiplication and by pulsed neutron techniques.

There were important differences between the mockup and the SEFOR reflector which had to be accounted for by both special measurements and calculations. In SEFOR removal of a rod leaves a large void. In the mockup, removal of the nickel plates left behind the steel ZPR-3 drawers and matrix. The reactivity effect of this steel was estimated by measuring the worth per unit weight of steel in the reflector after removal of the nickel.

A second important difference was the difference in materials outside the reflector. In SEFOR an aluminum structure followed by 2 in. of rods filled with B_4C and then by rods of serpentine lie beyond the reflector. In the mockup, only two drawers were available beyond the reflector at the position where the reflector worth was measured. The single-rod worth was measured first with no material outside the reflector except the steel matrix forming the two drawer locations (hence, effectively about 4 in. of 10% steel). A second measurement was then made with ¼ in. of $B_4^{10}C$ and one inch of polyethylene outside the reflector. The quadrant worth was measured only with the steel matrix outside the reflector. The aluminum structure outside the SEFOR reflector, together with structural aluminum webs between the SEFOR rods, was mocked up by aluminum plates in the reflector region of the mockup.

Other small differences in composition and geometry in the reflector, in the regions between the core and reflector, and in the core were present, but it is expected that these differences are treated adequately by calculation.

TABLE 6. Results of Measurements of 1-segment Reflector Worth

	Rod I	Rod II	Rod III	Average of Rods II and III
Nickel:				
total worth	100 ± 3¢*	127 ± 4¢*	93 ± 5¢*	110¢
Aluminum:				
worth/kg		0 82¢/kg*		
mass		17.9 kg		
total worth		14 7¢		13¢
Steel:				
worth/kg		0.46¢/kg*		
mass		39.2 kg		
total worth		18.0¢		16¢
Change in rod worth due to placing B_4C and polyethylene behind reflector		−6.2¢*		−5.4¢

* All starred values represent experimental results as reported in Ref. 1.

5.2. Experimental and Calculated Results of ZPR-3 Reflector Experiments

The experimental results for the 1-segment loading are given as the starred values in Table 6. The rod positions I, II, and III are indicated in Fig. 1. Rod positions II and III correspond to the positions for which calculations were made. Therefore, the results for rods II and III were averaged to obtain the experimental values that were compared with calculation. The large difference between rods II and III was caused by an asymmetric loading of plutonium in the 1-segment core, a situation that was corrected before the 2-segment reflector measurements were made.

TABLE 7. COMPARISON OF CALCULATED AND EXEPRIMENTAL VALUES FOR NICKEL IN REFLECTOR OF MOCKUP

	Calculated	Experimental
Worth of nickel in one rod		$1.10
Ratio: $\frac{\text{Worth of reflector quadrant}}{\text{Worth of one rod}}$	2.13	2.29
Ratio: $\frac{\text{Worth of total reflector}}{\text{Worth of quadrant}}$	3.58	
Calculated worth of nickel in total reflector	$9.45	
Extrapolated worth of nickel in total reflector = ($1.10) (2.29) (3.58)		$9.02

For the 2-segment core, the measured nickel worths in rods II and III were 120¢ and 121¢, respectively.

Calculated and experimental values for the nickel worth are compared in Table 7. The calculated values were based on the use of diffusion theory throughout the mockup, including the reflector region after removal of the nickel. The use of diffusion theory in the reflector region of the mockup was considered satisfactory for this purpose since a relatively large amount of steel and aluminum remained in the region after the nickel had been removed. The total nickel worth was calculated using 18 groups and one dimension (cylindrical). The ratios of one rod and one quadrant to the total worth were obtained by 4-group PDQ x,y calculations.

5.3. Methods of Obtaining SEFOR Reflector Worth from the ZPR-3 Results

The following two methods were used to evaluate the SEFOR reflector worth from the ZPR-3 experimental results:

(1) Direct Extrapolation Method—The experimental results were extrapolated to SEFOR, accounting for the differences between ZPR-3 and SEFOR compositions and dimensions. Calculated reflector worths enter this extrapolation only in the form of ratios, thereby reducing the uncertainties introduced by calculations.

(2) Boundary Condition Method—The reflector worth was calculated by replacing the void left by the withdrawn reflector and the shield outside the reflector with a calculated boundary condition. Calculations were made for the complete removal of the reflectors from both SEFOR and the ZPR-3. An approximate experimental value for this condition in the mockup was obtained by extrapolation of the ZPR-3 experimental measurements to the case for complete removal of reflector from the mockup. Comparison of this extrapolated experimental result and the calculation for ZPR-3 provided the required normalization for the SEFOR calculation.

5.3.1 Direct Extrapolation Method

The direct extrapolation method gave the following control worths for the 1- and 2-segment SEFOR designs:

Worth for 1-segment design = $10.2;
Worth for 2-segment design = $11.2.

Details of the extrapolation are given in Ref. 2.

5.3.2 Boundary Condition Method

The effect of the void left by the withdrawn SEFOR reflector rods was calculated by replacing the void and all regions outside the reflector with boundary conditions at the inside of the void region. Four-group one-dimensional (cylindrical) diffusion theory was used. The technique involved the calculation of leakage probabilities in a manner similar to that used by Oliver and Norman.[9]

The steps in calculating the boundary conditions were:

(1) The effective leakage probabilities across the void and escape probabilities from the void were calculated.
(2) A 4-group matrix albedo at the outer void surface was calculated.
(3) Ratios of exit to entering current densities at the inside of the void were calculated.
(4) Boundary conditions were calculated from the current densities using conventional diffusion theory.

The boundary condition method was applied both to SEFOR and to the mockup. The reactivity effect of removing all material from the mockup was extrapolated from the experimental results of Table 6.

The calculated values for the 1-segment core for both SEFOR and the mockup are given in Table 8.

TABLE 8. COMPARISON OF BOUNDARY CONDITION REFLECTOR CALCULATIONS WITH EXTRAPOLATED ZPR-3 MEASUREMENTS FOR THE 1-SEGMENT CORE

Description	Calculated, $	Extrapolated from Measurements, $ (All material removed from reflector region)
SEFOR	10.2	—
Mockup with B_4C and polyethylene behind reflector	9.9	10.9
Mockup with 10 cm of 10% steel behind reflector	10.7	11.4

The values for the mockup extrapolated from the experimental data are also given in the table.

Normalization of the calculated results of Table 8 to the experimental values gives a predicted value of \$11.1 for the 1-segment SEFOR core. This value is 8% higher than the value of \$10.2 obtained from the direct extrapolation method.

An approximate calculation of the 2-segment reflector worth in the mockup was made by homogenizing the gap material with the fuel for the radial calculation. This resulted in increased radial leakage and a 5% increase in reflector worth, which compares with a measured increase of 9%. The 5% calculated increase gives a reflector worth of \$11.6 for the 2-segment SEFOR core, which is 4% higher than the value obtained from the direct extrapolation method.

The effect on reflector strength of placing an absorber and hydrogeneous moderator behind the reflector is predicted qualitatively. The B_4C and polyethylene behind the reflector in the mockup reduced the reflector worth by 5%, which compares to the calculated reduction of 8%. The use of the 10 cm of 10% steel behind the reflector to mock up the ZPR-3 matrix may be inaccurate; to check the sensitivity of this assumption the reflector worth was also calculated with 20 cm of 10% steel. This gave a worth of \$10.2, to be compared with the \$10.7 value in Table 8.

The details of the method for calculating the boundary conditions are given in Ref. 2.

6. Doppler Coefficient

Experiments were performed in the mockup to help determine the magnitude of the SEFOR Doppler coefficient. The results showed close agreement between calculation and experiment for the U^{238} Doppler coefficient and a near-zero contribution by Pu^{239}, results which are consistent with earlier ZPR-3 measurements.[10] Applying the same techniques for the U^{238} Doppler calculation for SEFOR and assuming a zero contribution from Pu^{239}, the calculated Doppler coefficient for the SEFOR 2-segment design is $T(dk/dT) = -0.0085$. This value is well above the value of -0.004 used for SEFOR safeguard analyses.

6.1. Experimental Procedure and Results

The ZPR-3 measurements were performed by the "hot sample-cold reactor" technique[10] in which a heated sample is exchanged with an equivalent cold sample and the difference in steady-state reactivities is measured. Measurements were made for $U^{238}O_2$ samples and for 12.5% PuO_2-87.5% $U^{238}O_2$ samples. Measurements for the $U^{238}O_2$ sample were later repeated with sodium removed from the regions surrounding the samples. Measurements were made for sample temperatures of 300°K, 500°K, 800°K, and 1100°K.

The results of the measurements with sodium present are shown in Fig. 8 with reactivity per kilogram U^{238} plotted against $\ln (T/T_0)$. The $U^{238}O_2$ results are plotted as measured. The 12.5% PuO_2-UO_2 measured values are shown also plotted on a $\delta k/k$ per kilogram U^{238} basis, assuming a zero contribution from the plutonium. The fact that the results are indistinguishable from the results for the pure UO_2 samples forms the basis for the assumption that the plutonium contribution to the SEFOR Doppler coefficient is negligible.

A straight line through the experimental points in Fig. 8 represents a T^{-1} variation of the Doppler coefficient, dk/dT (i.e., $T(dk/dT) = \text{constant}$). The solid line in Fig. 8 represents the T^{-1} variation drawn through the high-temperature points which correspond to the fuel temperatures of most interest to the SEFOR experimental program. The dashed line represents a $T^{-0.9}$ variation. Although it is possible to construct a T^{-1} line that lies within the experimental error at each temperature, the $T^{-0.9}$ curve provides a better fit. Although the data are insufficient to establish the temperature variation accurately, it is interesting to note that the calculated temperature variation that best fits the calculated SEFOR isothermal Doppler coefficient from 300°K to 5000°K is $T^{-0.9}$.*

6.2. Comparison of Calculated and Experimental Values

The calculated Doppler effect of the heated sample was based on a U^{238} temperature rise from 700°K to 1400°K. From Fig. 8, the experimental value corresponding to this temperature change is -1.5×10^{-5} $\delta k/k$/kg U^{238}.

The calculated reactivity effect for a U^{238} temperature change from 700°K to 1400°K was also -1.5×10^{-5} $\delta k/k$/kg U^{238}. The calculated value for the Doppler effect of the heated sample was obtained by perturbation theory using a two-dimensional 16-group CRAM problem. The change in U^{238} absorption cross section ($\delta\sigma_a$) below 4 keV was calculated by the

*The calculated temperature variation of the U^{238} Doppler coefficient in SEFOR was obtained from the following 18-group spherical calculations in which the U^{238} fuel temperature was assumed constant throughout the core and represented the only change between problems:

U^{238} Temperature, °K	Criticality Factor
300	1.04804
700	1.03983
1400	1.03245
3000	1.02389
5000	1.01804

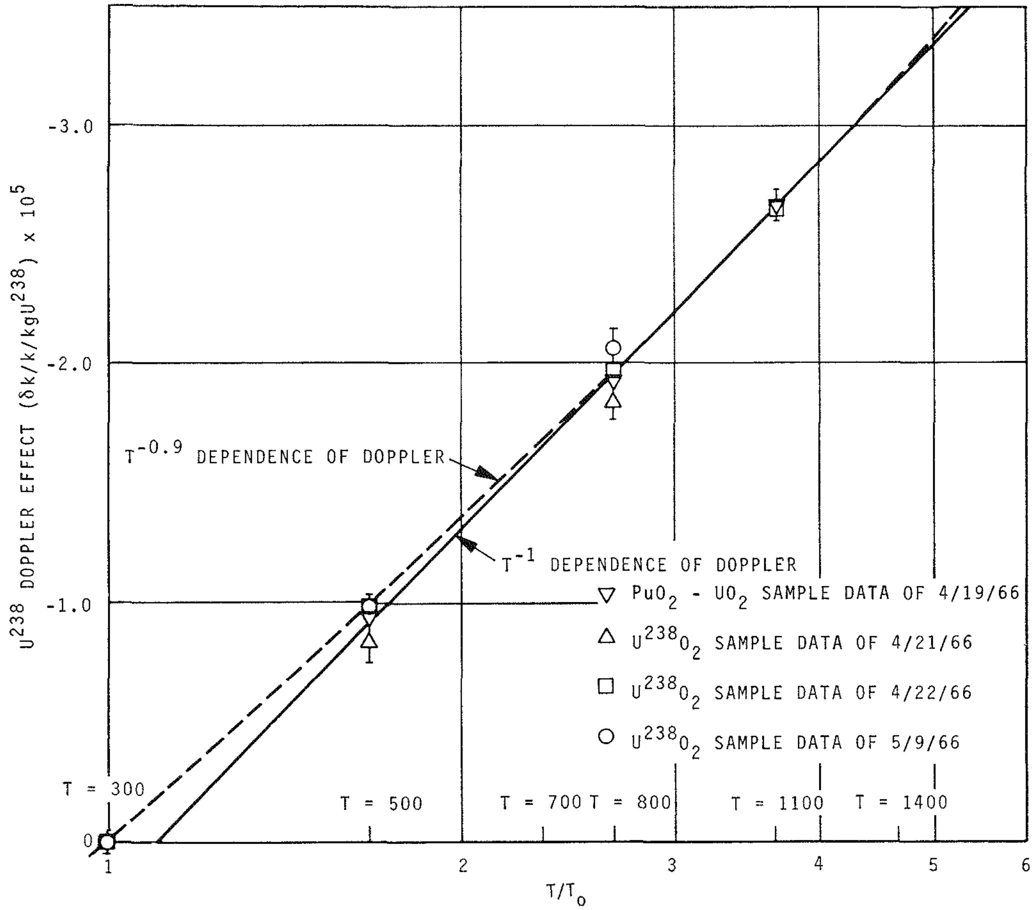

FIG. 8. U^{238} Doppler Measurements in SEFOR Mockup in ZPR-3. (Temperatures in °K)

RAPTURE code[11] using recent Columbia resonance parameters.[12] For the unresolved resonances (>4 keV), the results of Greebler and Goldman[13] were used (which were also based on the use of RAPTURE). Values of $\delta\sigma_a$ were calculated for the case in which both the absorber and the surrounding medium are at the same temperature. The SEFOR potential cross sections, σ_p, which were nearly equal to the ZPR-3 values, were used for the initial, uncorrected calculation.

A correction was made in the calculation to account for the fact that only the sample was heated while the surrounding medium remained at room temperature. A rough estimate by Greebler for an effective potential scattering cross section for U^{238} to account for this effect was 54 b, compared to 37 b calculated for SEFOR. Using the 54-b value for the heated sample increases the calculated U^{238} Doppler effect by about 1%, indicating that the net small sample correction is low.*

* The net correction is small because the magnitude of the Doppler effect is decreased by the larger value of σ_p above 1 keV and increased below 1 keV.

The agreement between theory and experiment is tempered by the recognition that uncertainty remains concerning the accurate interpretation of the experiment, and that all known refinements have not been included in the Doppler calculations. For example, interference effects were not included, which may be a correction of the order of 10%. Hence, it is not our purpose to emphasize the close agreement between calculation and experiment. It is our purpose, however, to show sufficient agreement between calculation and experiment to assure the validity of the conclusion stated in the initial paragraph of this section, namely, that the calculated SEFOR Doppler coefficient is significantly larger in magnitude than the value used for SEFOR safeguards analyses.

6.3. *Effect of Loss of Sodium on Doppler Coefficient*

Loss of sodium results in hardening of the spectrum and an accompanying reduction in the Doppler coefficient. The U^{238} Doppler effect was measured in the mockup with sodium removed from a large enough area

TABLE 9. REDUCTION IN DOPPLER COEFFICIENT FROM LOSS OF SODIUM

Sodium Volume Fraction	Fractional Reduction, %	
	Calculated	Experimental
0.244	9.6	
0.280	12.4	
0.303		17.5

around the sample to obtain a spectrum characteristic of the reactor with sodium removed.

As shown in Table 1, the sodium volume fraction mocked up in ZPR-3 was 30.3%. The reduction in Doppler coefficient due to loss of sodium was calculated for earlier SEFOR designs containing sodium volume fractions of 24.4% and 28.0%.

The experimental and calculated results for the reduction in Doppler coefficient from loss of sodium are listed in Table 9. Use of the measured 17.5% value would reduce the SEFOR Doppler coefficient $[T(dk/dT)]$ from −0.0085 to −0.0070.

7. Sodium-loss Reactivity

7.1. Sodium Loss from Center of Core

The calculated value for the maximum positive reactivity from loss of sodium from the center of the

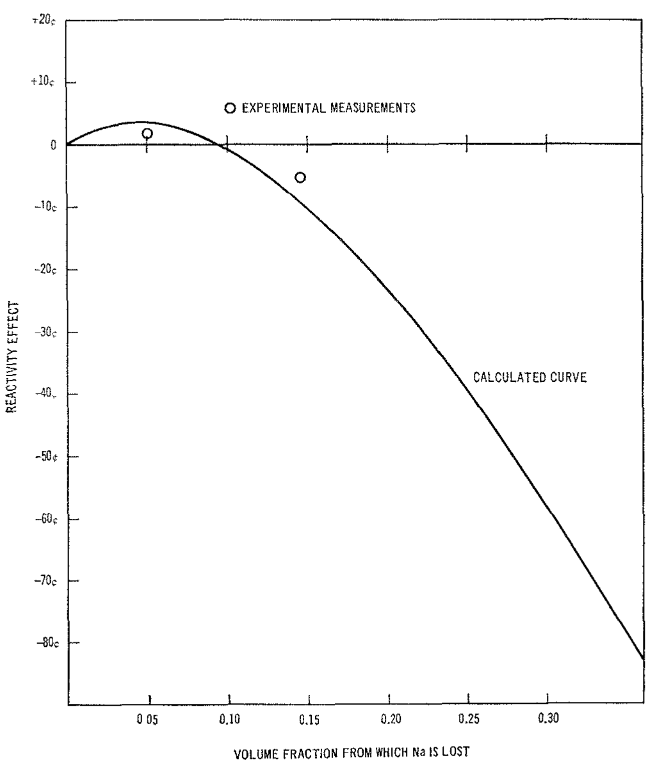

FIG. 9. Measured and Calculated Sodium-loss Reactivity.

SEFOR core was +3¢. This value was low enough to indicate that this reactivity effect does not pose a safety problem for SEFOR. To verify this expectation, the maximum positive reactivity due to sodium loss was measured in the mockup.

The reactivity effects of complete removal of sodium from the central 5, 10, and 15 v/o of the 1-segment core were measured. The maximum measured positive effect was +6¢, which occurred with sodium removed from the central 10% of the core. The sodium-loss reactivity became decidedly negative with removal from the central 15% of the core.

The calculated values together with the three experimental points are plotted in Fig. 9.

In the ZPR-3 measurements, the voided zone was distributed uniformly around the center of the core only in the 10% measurement; the voids were slightly displaced for the 5% and 15% measurements. Had they also surrounded the core center uniformly, it is expected that the experimental results for these points would have been slightly more positive. However, it is concluded from the experiments that the +6¢ at 10% sodium loss is close to the maximum positive effect and that the effect becomes strongly negative when more than 13% of the volume is voided.

7.2. Sodium Loss from the Gap

Since the 2-segment design has been selected for SEFOR, it was useful to establish experimentally that the loss of sodium from the gap would not cause an additional large positive reactivity. This was done by adding sodium to the gaps of 63 central drawers (which is one-third of the drawers in that half of the mockup). The resulting reactivity was positive, +1.1¢/kg of sodium added. Hence, loss of sodium from the gap would be negative.

7.3. Calculational Method

Spherical geometry was used for sodium-loss calculations in order to maximize the positive effect and to avoid the use of transverse bucklings. The sodium-loss effect has two principal components—a large positive component due to hardening of the spectrum, and a large negative component due to increased leakage. The former component has its maximum influence and the latter component its minimum influence when sodium is lost from the center of the core. Hence, the maximum positive net effect should occur when sodium is lost from a small spherical region around the center of the core. In addition, there is a smaller positive effect caused by the absence of capture by the removed sodium.

The calculated reactivities for sodium loss as a function of fraction of the core voided are listed in Table

10. In addition, an approximate breakdown of the components which make up this reactivity effect are listed. It is observed from Table 10 that the small maximum positive effect is the sum of large positive and negative components. For this reason, the agreement between theory and experiment shown in Fig. 9 is gratifying.

8. Ratio of Prompt-neutron Lifetime to Effective Delayed-neutron Fraction

8.1. Experimental Results

The ratio l/β_{eff} was measured by the pulsed neutron technique and by noise analysis using cross correlation. The pulsed neutron measurements were reported by Brunson.[14] The noise analysis was reported by Morrell.[15] Extrapolating the results in References 14 and 15 to the critical reactor gives for the two methods:

Pulsed neutron: $l/\beta_{eff} = 2.05 \times 10^{-4}$ sec;

Noise analysis: $l/\beta_{eff} = 2.05 \times 10^{-4}$ sec.

The experimental error in these numbers is of the order of 5%. For the calculated value of β_{eff} of 0.0033 (see below) and the experimental value of l/β_{eff}, the lifetime is 0.68 μsec.

This noise measurement represented the first application of the cross-correlation technique to a fast reactor. The agreement with the pulsed neutron result has led to the recommended use of noise analysis to measure l/β_{eff} in SEFOR.

8.2. Calculated Value of β_{eff}

The calculated value of β_{eff} for the SEFOR mockup is 0.0033. Delayed-neutron parameters for fast fission recommended by Keepin[16] were used. β_{eff} is dependent both on the relative number of fissions between U^{238} and Pu^{239} and on the relative effectiveness of delayed versus prompt neutrons. The relative number of fissions was calculated using cross sections which gave reasonably good agreement with the measured U^{238}/Pu^{239} fission ratio (see Sect. 9 below). Approximately 12% of the fissions in the mockup occur in U^{238}. The relative effectiveness of delayed neutrons to prompt neutrons, β_{eff}/β, is 0.91, and this result is essentially the same for each delayed-neutron group.

8.3. Calculated Value of Prompt-neutron Lifetime

The lifetime calculation for the SEFOR mockup is reported in Ref. 4. Using a two-dimensional 16-group CRAM calculation and using cross sections almost equivalent to ours, Greebler *et al.* obtained $l = 0.65$ μsec. Using the SEFOR mockup 60-group cross sections and one-dimensional radial calculations, we obtained $l = 0.54$ μsec; however, it is known that the one-dimensional result is sensitive to the transverse bucklings used. Calculated values were obtained from the calculated reactivity effect of a $1/v$ absorber.

TABLE 10. Calculation of Sodium-loss Reactivity

Voided Zone		Reactivity ($)			
Relative Radius (r/R_0) to which Sodium is Voided	Fraction of Volume Voided, %	Total	Leakage Component	Spectrum Component	Sodium Capture Component
0.4	6.4	+0.03	−0.43	+0.41	+0.05
0.5	12.5	−0.05	−0.92	+0.78	+0.09
0.6	21.6	−0.28	−1.70	+1.26	+0.16
0.7	34.3	−0.76	−2.86	+1.87	+0.23
1.0	100	−4.4	−8.7	+3.7	+0.6
Vessel	—	−10.1	−15.6	+4.9	+0.6

For $l = 0.65$ μsec, the calculated value of l/β_{eff} is 1.96×10^{-4} sec, which is close to the experimental values. The 0.54-μsec lifetime gives an l/β_{eff} value 20% below the experiment.

9. Reaction Parameters

9.1. Reaction Ratios

Relative fission rates of U^{235}, U^{238}, Pu^{239}, and Pu^{240} were measured at the core center by means of fission counters. In addition, U^{235} and U^{238} foils were irradiated at the center and analyzed radiochemically at Argonne to determine the ratios of the U^{238} capture and fission rates to the U^{235} fission rate.

The measured reaction rates relative to the Pu^{239} fission rate are given in Table 11. The radiochemical results were normalized to the Pu^{239} fission rate by multiplying by the fission-counter-measured U^{235}/Pu^{239} fission ratio. Values listed are ratios of reaction rate per atom; hence, they can be compared to the calculated ratios of the quantity $\int \sigma(E)\Phi(E)\,dE$. Calculated values are also listed in Table 11. SEFOR-mockup 18-group cross sections were used for the calculations; hence, the Pu^{239} cross sections were self-shielded and the U^{235} were infinitely dilute.

TABLE 11. Central Reaction Ratios

Ratio	Experimental Technique	Measured	Calculated
$\sigma_f(U^{235})/\sigma_f(Pu^{239})$	fission counter	1.09	1.15
$\sigma_f(Pu^{240})/\sigma_f(Pu^{239})$	fission counter	0.219	0.183
$\sigma_f(U^{238})/\sigma_f(Pu^{239})$	fission counter	0.029	0.028
$\sigma_f(U^{238})/\sigma_f(Pu^{239})$	foil irradiation (radiochemical)	0.026	
$\sigma_c(U^{238})/\sigma_f(Pu^{239})$	foil irradiation (radiochemical)	0.150	0.143

The U^{238}/Pu^{239} ratios are in agreement; the U^{235} and Pu^{240} values are not as close. Better agreement is obtained for the U^{235}/Pu^{239} fission ratio by using infinitely dilute Pu^{239} cross sections (1.08 instead of 1.15), but the self-shielded value is probably more appropriate and its use leads to better agreement elsewhere.

9.2. Reaction-rate Traverses

Fission-rate traverses were made using U^{238} and Pu^{239} fission counters. A boron absorption-rate traverse was made with a BF_3 chamber. The shape of the traverses in the x direction (radial or axial) were compared with calculated traverses using eighteen energy groups.

The measured and calculated radial Pu^{239} fission traverses at the midplane of the 2-segment loading are plotted in Fig. 10. Axial Pu^{239} and U^{238} fission traverses and the axial boron-absorption traverse for the 2-segment mockup are shown in Figures 11–13. In each case the curves were normalized so that the spatial integrals $\int \sigma \Phi dV$ over the core were equal for the experimental and calculated curves. For the Pu^{239} traverses, self-shielded Pu^{239} cross sections were used in the fuel regions; infinitely dilute cross sections were used in nonfuel regions.

Use of the region-dependent cross sections provided good agreement for the radial Pu^{239} traverse. Peaking in and near the gap in the axial traverses was underestimated. It is likely that this underestimate results from the use of diffusion theory; in fact, Helm *et al.*[17] reported similar underestimates of peaking near boundaries for traverses in ZPR-6 using diffusing theory and agreement using transport theory.

9.3. Pu^{239} Worth Traverse

An axial Pu^{239} reactivity worth traverse was made in the 2-segment core with a 24.09-g sample of Pu^{239}. The relative calculated and measured distributions are

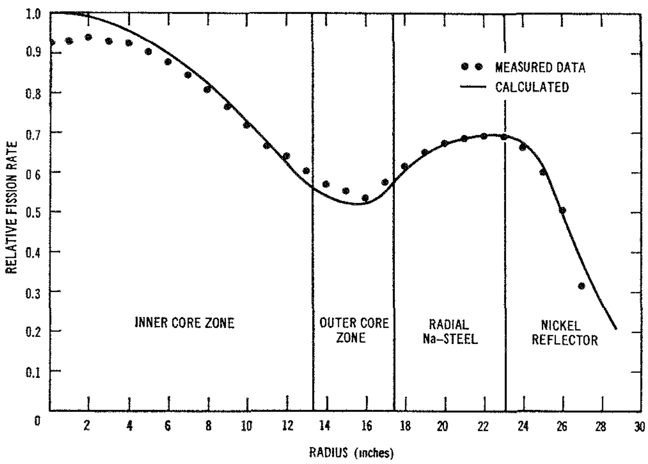

FIG. 10. Radial Pu^{239} Fission Traverse.

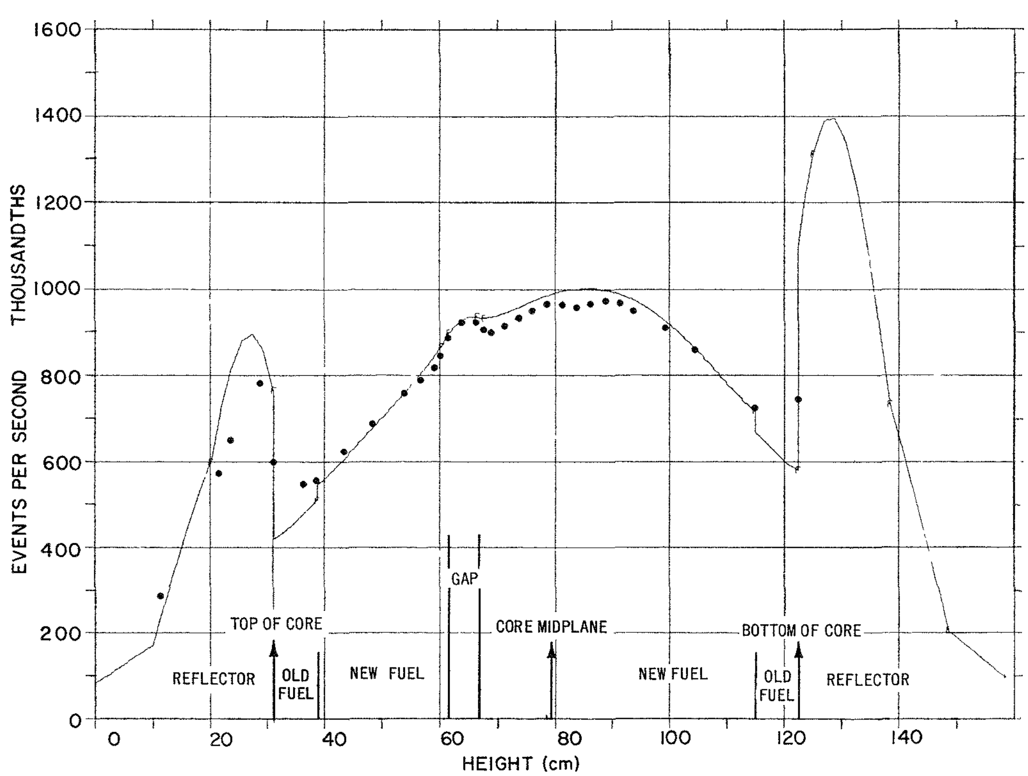

FIG. 11. Axial Pu-239 Fission Traverse.

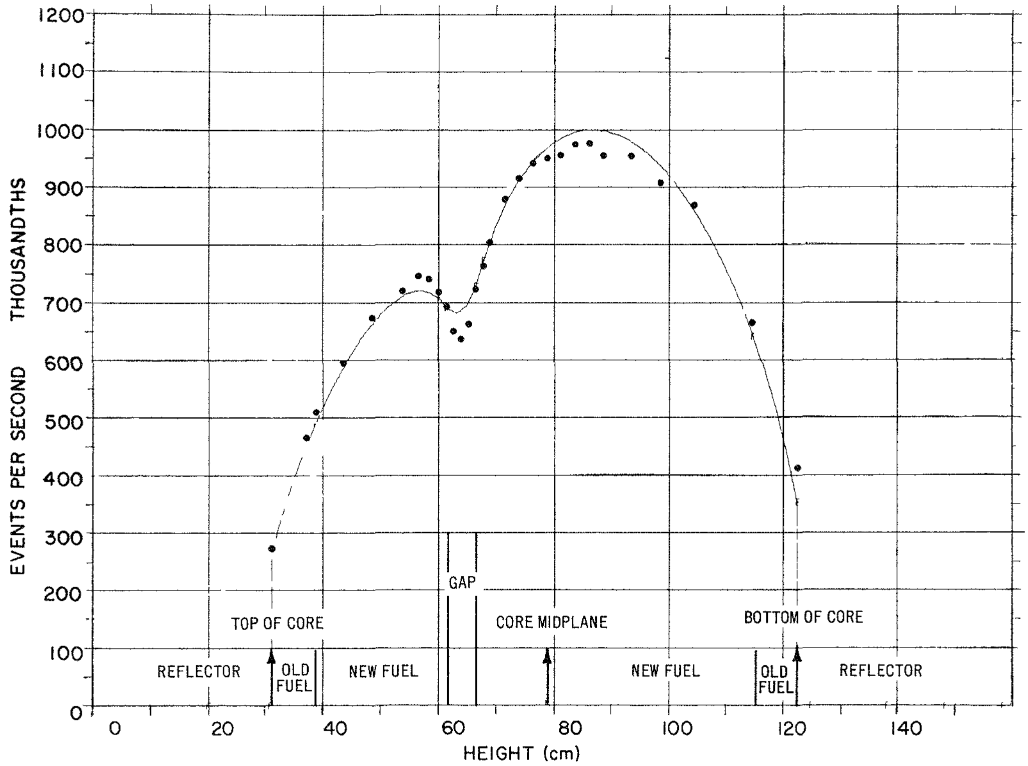

Fig. 12. Axial U-238 Fission Traverse.

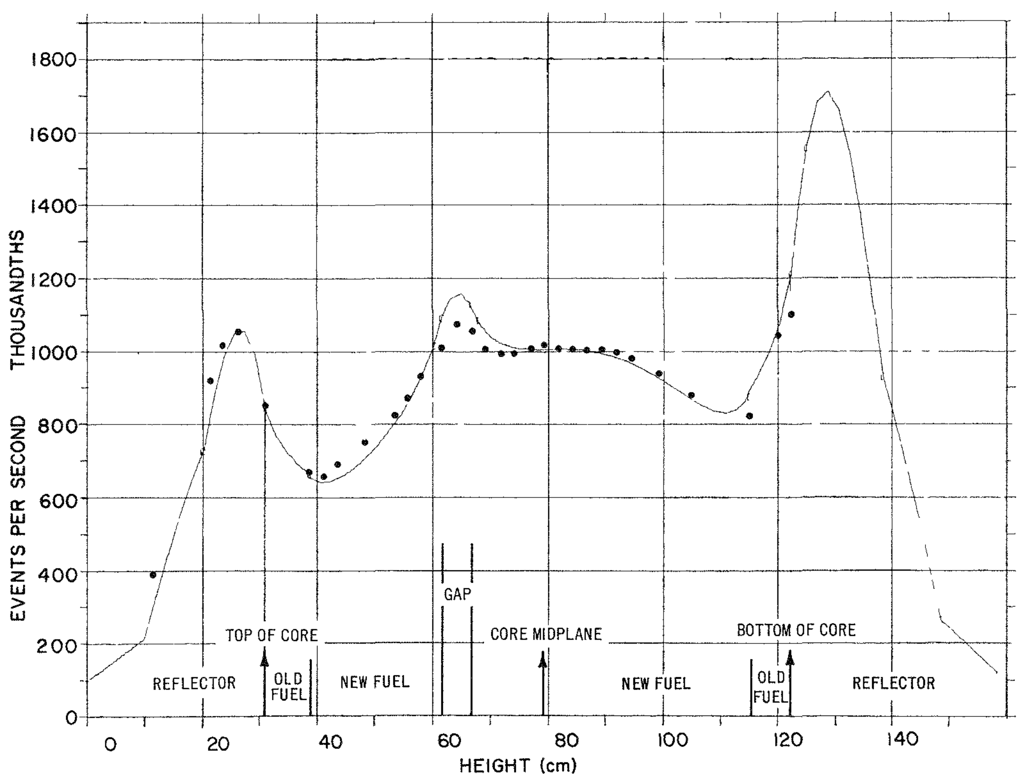

Fig. 13. Axial Boron-absorption Traverse.

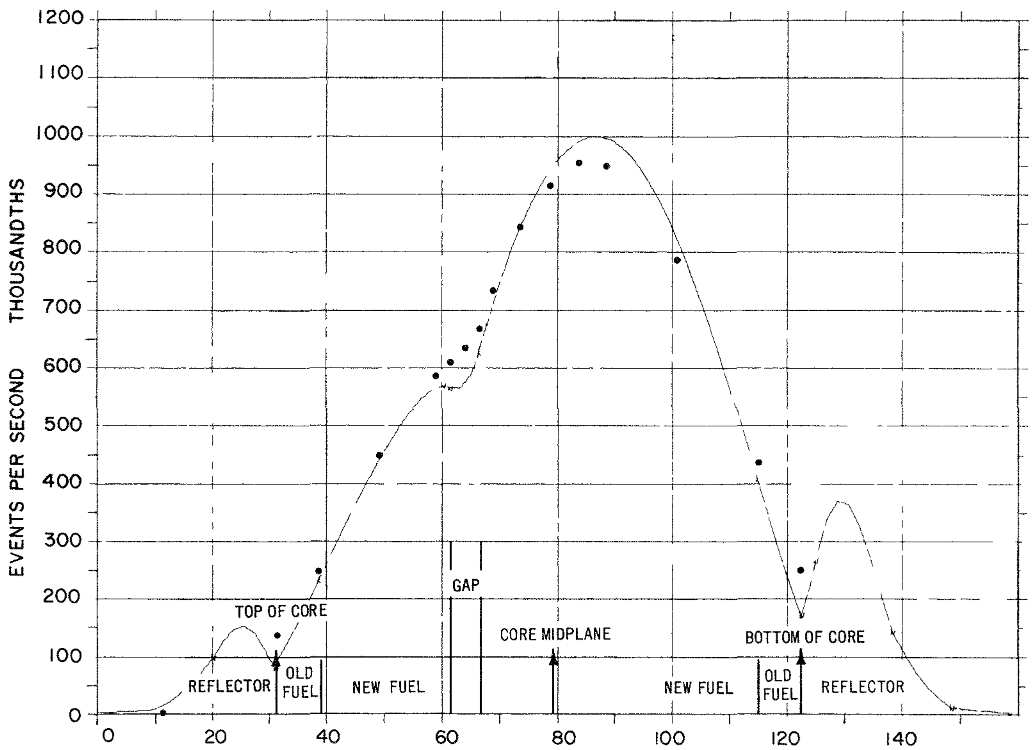

FIG. 14. Axial Pu-239 Worth Traverse.

shown in Figure 14 normalized to equal areas under the curves in the core.

The calculated distribution was obtained from the expression

$$\sum_j \left[\sum_i \nu_i \sigma_{f,i}(z)\phi_i(z)\right]\chi_j\phi_j^*(z) - \sum_i \sigma_{ai}(z)\phi_i(z)\phi_i^*(z),$$

where the summations are over the eighteen groups.

As was the case for the fission traverses, the agreement is fair, but the worth in the gap is underestimated.

REFERENCES

1. R. L. McVean, R. W. Goin, A. Weitzberg, A. Leridon, and J. A. Kremser, *Critical Assembly Mockup ofthe SEFOR Reactor in ZPR-3*, See Paper in Session VI of This Conference; Also ANL-7248, to be published.
2. A. B. Reynolds and S. L. Stewart, *Analysis of the SEFOR Mockup Experiments in ZPR-3*, GEAP-5294 (to be published).
3. B. Wolfe, K. Hikido, K. M. Horst, and A. B. Reynolds, *SEFOR—A Status Report*, ANS-100, Fast Reactor Technology National Topical Meeting, Detroit (April 1965).
4. J. K. Long, R. L. McVean, A. B. Reynolds, S. L. Stewart, A. Weitzberg, and A. Leridon, "Critical Mass of SEFOR Mockup in ZPR-3," Nucl. Sci. Eng., **25,** 442 (1966).
5. P. Greebler, G. L. Gyorey, B. A. Hutchins, and B. M. Segal, *Implications of Recent Fast Critical Experiments on Basic Fast Reactor Design Data and Calculational Methods*, See Paper in Session II of This Conference.
6. J. K. Long *et al.*, "Fast Neutron Power Reactor Studies with ZPR-3," *Proc. Second United Nations International Conference on the Peaceful Uses of Atomic Energy*, Geneva, **12,** 119, (1958).
7. P. Greebler, C. L. Cowan, C. L. Fies, G. L. Gyorey, and J. R. Sueoka, *Critical Physics Parameters and Their Uncertainties in a 1000-MWe Fast Ceramic Reactor*, General Electric, San Jose, International Conference on Safety, Fuels, and Core Design in Large Fast Reactors, at Argonne National Laboratory (1965).
8. G. I. Bell, Nucl. Sci. Eng., **5,** 138 (1959).
9. D. G. Oliver and R. H. Norman, Trans. Am. Nucl. Soc., **8,** 203 (1965).
10. G. J. Fischer, D. A. Meneley, R. N. Hwang, E. F. Groh, and C. E. Till, Nucl. Sci. Eng., **25,** 37 (1966).
11. J. H. Ferziger, P. Greebler, M. D. Kelley, and J. W. Walton, *Resonance Integral Calculations for Evaluation of Doppler Coefficients—the RAPTURE Code*, GEAP-3923 (July 1962).
12. J. Garg, J. Rainwater, J. S. Petersen, and W. W. Havens, Jr., Phys. Rev., **134,** B985 (1964).
13. P. Greebler and E. Goldman, *Doppler Calculations for Large Fast Ceramic Reactors—Effects of Improved Methods and Recent Cross-section Information*, GEAP-4092 (Dec. 1962).
14. G. S. Brunson and R. J. Huber, Trans. Am. Nucl. Soc., **9,** 168 (1966).
15. R. P. Morrell, *SEFOR β/l Measurements by Noise Analysis Techniques*, PTR-809 (June 1966).
16. G. R. Keepin, *Physics of Nuclear Kinetics,* Addison-Wesley, Reading, Mass. (1965).
17. F. H. Helm, A. Ancarani, and A. Karam, Trans. Am. Nucl. Soc., **9,** 228 (1966).

Discussion

Mr. Gandini (CNEN): You mentioned that if you remove sodium in the vicinity of the sample you lose about 17% of your negative Doppler coefficient. Is the amount of sodium which you remove large or small? Removal of a small quantity will give different results from removal of a large quantity.

Mr. Reynolds: That's right. This is the effect of removing all of the sodium from the center of the core for the volume mentioned.

Mr. Kohler (Texas A&M): On the basis of the measurements for the control rods in the reflector, did you decide that you don't have to have in-core control rods in your final design?

Mr. Reynolds: Yes, we are sure now that we shall not have to make provisions for that because we have sufficient reactivity control margins.